Origami metamaterials : design, symmetries, and combinatorics

Dieleman, P.

CHAPTER 4

RATIONAL DESIGN OF ORIGAMI PATTERNS

4.1 Introduction

In the previous chapters we showed that by converting the problem of rigid foldability into a discrete tiling problem, we can fully characterize and count all the possible crease patterns which can be made using a single vertex, its supplement, and their two mirror images. Doing so we uncovered new, space-filing periodic tilings –e.g. the tiling in Fig. 3.1– as well as a vast array of aperiodic tilings.

In this section we aim to rationally design origami patterns using the same discrete tiling strategy. We first show that we can create periodic or non-periodic crease patterns, starting from a periodic class-I tiling in section 4.2. Then we focus on class-I patterns, which allow the greatest design space of the four different classes, as the number of class-I patterns ($N_{\mathrm{t}}^{\mathrm{I}} = 8 \cdot (2^m - 1) \cdot (2^n - 1)$) scales exponentially with both m and n. In section 4.3 we show how to program class-I patterns such that we obtain strips that can be folded into shapes with a pre-programmed curvature. In section 4.4 we then show how to extend this design strategy to $m \times n$ sheets, which can be folded into two different, pre-programmed shapes. The result is a multishape material – this is unique for origami, where one usually designs structures with only one target shape in mind. Finally, we show experimental realizations of such multishape sheets, in the form of lasercut Mylar™ sheets.

4.2 Space-Filling Tilings

In this section we will address the issue of space-filling tilings, where we will focus specifically on class-I patterns. The first requirement for a crease pattern to be space-filling is for its corresponding tile pattern to be space filling. In Fig. 4.1.A we show a tile-pattern of which the top and bottom fit together, but the left and right side do not – this pattern therefore can not be turned into a space-filling crease pattern. In Fig. 4.1.B we replaced the leftmost columns with tiles which create a space filling tile pattern.

In Fig. 4.2.A we convert the 4×4 pattern of Fig. 4.1.B into a 12×12 crease pattern using nine unit cells. To do so, we fix 11 degrees of freedom: the crease lengths $\{t_i\}$ and $\{l_i\}$ (8 d.o.f.) and the sector angles $\{\alpha_i\} = \{60°, 90°, 135°, 75°\}$ (3 d.o.f., as $\sum \alpha_i = 2\pi$). We can clearly see that the resulting pattern is not space-filling. This is because the lengths of the top and left side of the crease pattern, do not match those of the bottom and right side. To ensure matching lengths, we require that $b_i = t_i$ and $r_i = l_i$; fixing $\{\alpha_i\}$. These yield eight equations for the eight degrees of freedom $\{t_i\}$ and $\{l_i\}$. We solve these nonlinear coupled equations numerically (by means of a Python script with standard minimization libraries, scipy.optimize.minimize, using the Nelder-Mead method). The result is shown in Fig. 4.1B, yielding a periodic, space filling crease pattern.

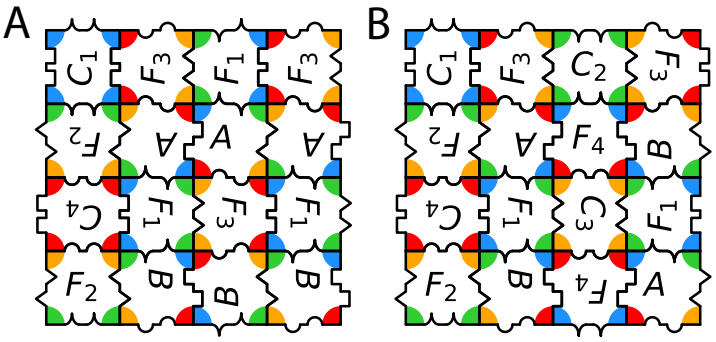

FIGURE 4.1: (A) A class-I pattern that does not tile the plane: although the top and bottom side of this tiling fit together, the left and right side do not. (B) A class-I pattern which tiles the plane, and can potentially also tile the plane once converted into a real-space crease pattern, see Fig. 4.2.

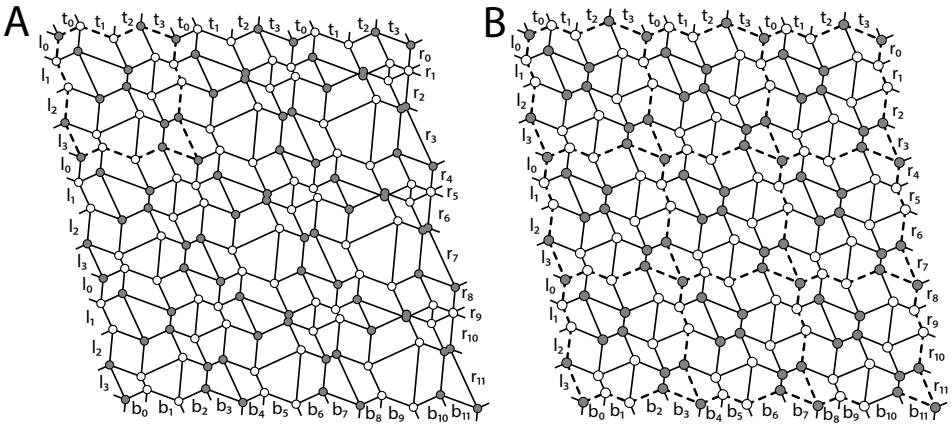

FIGURE 4.2: (A) Real space version of the tile pattern shown in Fig. 4.1, where the lengths of the top (t_i), and the left side (l_i) are not specifically tuned, which leads to a non-space filling pattern. (B) Real space version of the tile pattern shown in Fig. 4.1b, where the lengths of the top (t_i), and the left side (l_i) are tuned such that the pattern is space-filling. Dashed lines indicate unit cells. Both patterns have $\{\alpha_1, \alpha_2, \alpha_3, \alpha_4\} = \{60°, 90°, 135°, 75°\}$ for the unsupplemented vertex (indicated in white).

4.3 Designing Origami Strips with One Target Shape

In this section we will show that we can design one of the two folding-branches of a class-I tiling in such a way such that it folds into a sheet with a predefined curvature along one direction. The other folding branch folds into a cylinder. To illustrate how we construct origami patterns which lead to certain predefined shapes, we depicted an $m = 13$, $n = 5$ class-I tiling in Fig.4.3.A. The columns in this pattern consist solely of A-tiles, B-tiles, or F_i-tiles, and have a periodicity of 2 in the vertical direction. The colors purple and orange in this figure indicate curvature for the non-cylindrical folding branch. Here purple indicates the sheet curving upward, and orange indicates the sheet curving downward (or vice versa). This is demonstrated in Fig.4.3.B, where a realization of the tiling of Fig.4.3.A is shown with sector angles $\alpha_i = \{60°, 75°, 120°, 105°\}$, which is the base vertex used for all the subsequent crease patterns in this section. This corresponds to a flat foldable vertex, but one our approach works equally well for generic vertices. The red lines indicate mountain folds, whereas

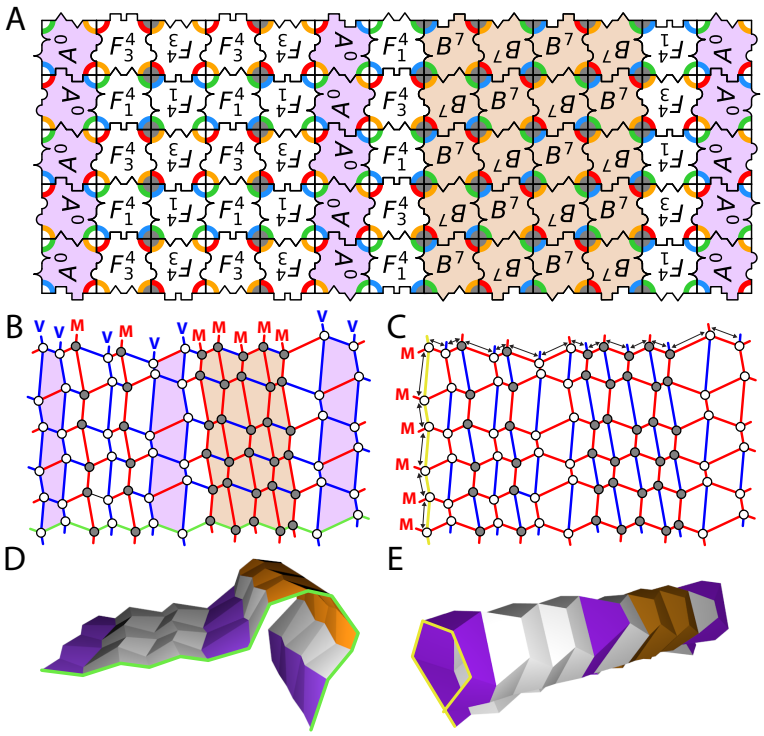

FIGURE 4.3: (A) Class-I tiling, with columns consisting out of bricks with identical letters. Purple columns contain A-tiles, whereas orange columns contain B-tiles. These determine the curvature of the pattern when folded along the vertical direction, see (B,D). (B) MV pattern associated with the pattern in (A), when folded along the vertical direction. (C) MV pattern associated with the pattern in (A), when folded along the horizontal direction. (D,E) 3D shapes of folded states of the patterns depicted in (B,C) were calculated using software from [63].

the blue lines indicate valley folds. A 3D visualization of this pattern is depicted in Fig.4.3.D, showing that we can adjust the curvature of the sheet by programming the sequence of bricks in the horizontal direction.

We see that the purple columns, consisting out of A-tiles, are lined left and right by valley folds (V). On the contrary, we see that the orange columns, consisting out of B-tiles, are lined left and right by mountain folds (M). Consecutive columns of B tiles, such as in the middle of the

pattern, therefore induce a downward curvature, whereas consecutive columns of A-tiles induce a positive curvature (or the other way around, as every MV-pattern has a mirrored counterpart). Furthermore we notice that the F-tiles always have opposite fold signs left and right. Multiple adjacent columns of F-tiles do not induce curvature, but form a corrugated sheet, like many origami patterns do (such as Miura-ori). Lastly, we observe from Fig.4.3.A that when mixing F tiles with A and B tiles, an even number of consecutive F-tiles is surrounded left and right by the same kind of tile (either A or B), this can be seen in column 2–5 in Fig.4.3.A. An odd number of consecutive F-tiles is surrounded left and right by both an A-tile and a B tile.

Altogether we then see that class-I tilings can be used to program any arbitrary code of fold signs along the vertical (or horizontal) direction. We do this by choosing the right combination of A, B, and F-tiles. In this case the pattern can be written as,

$$VVMVMVVMMMMMVV. \tag{4.1}$$

Different combinations of tiles can result in nearly any of the 2^{m+1} different patterns, where n is the number of columns of tiles. The only patterns that can not be created within class-I itself are the ones where mountains and valleys alternate throughout the sheet ($VMVM\ldots$). The corresponding tiling would be comprised solely of F tiles, and therefore is not a class-I, but a class-III tiling. The total number of possible MV patterns that we can choose from is therefore,

$$2^{m+1} - 2. \tag{4.2}$$

Using the design strategy of alternating columns (or rows) of A, B, and F-tiles ensures that one of the two branches still folds into a cylinder, which is shown in the MV pattern of Fig.4.3.C, and the 3D visualization of Fig.4.3.E. Note that the left edge of the pattern in Fig.4.3.C is colored green, corresponding to the green edge in Fig.4.3.E. In the next section we will show that we can also modify this cylindrical folding branch, by adding C tiles.

First however, we will extend on the principle of using A and B-tiles to introduce curvature into certain places to target a more complicated shape. In Fig.4.4.A we show a 67 by 4 vertex quadrilateral mesh, converted from a 66 by 3 tile pattern. Note that here we count the *internal* vertices and

internal tiles, as we can arbitrarily reshape the quadrilaterals on the edge of the this pattern without affecting the folding motion. Fig.4.4.B reveals that the mesh depicted in Fig.4.4.A folds into the Greek-letter β. Note that the green edge in Fig.4.4.A corresponds to the green edge in Fig.4.4.B. We designed the pattern in Fig. 4.4.A to consist of flat areas when folded, corresponding to columns of F-tiles. These are interspersed with A and B-tiles to create curves with varying radius of curvature. For example, the ratio of B to F columns in the top loop of the β is $1:2$, whereas the ratio of B to F tiles in the bottom loop of the letter β is $1:4$. The resultant 3D shape therefore shows that the radius of curvature of the bottom loop is approximately twice as big as the radius of curvature of the top loop, throughout the folding motion of the sheet. This can also be seen in Fig.4.5. Here several snapshots of the crease pattern depicted in Fig.4.4.A are taken throughout its folding motion, as seen from the side. Note that the folding motion is restricted, as eventually the sheet comes into contact with itself. In principle this strategy –varying the ratio of A and B to F-tiles– can be

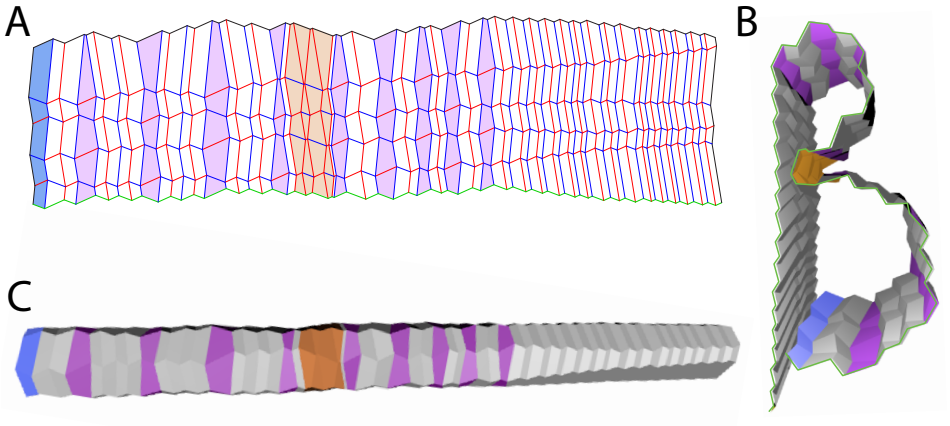

FIGURE 4.4: (A) A 67 by 4 (internal) vertex quadrilateral mesh, which is a realization of 66 by 3 internal tile pattern (not shown here). By choosing the position of the A, B, and F tiles we can program the curvature of the sheet when folded. (B) 3D visualization of the MV pattern depicted in (A), revealing this mesh folds into the shape of the letter β. (C) 3D visualization of the mesh shown in (A) when folded into the cylinder configuration (MV pattern not shown here). 3D folded shapes in figures (B,C) calculated using software from [63].

extended to achieve any kind of ratio between the curved parts of the 3D shape. Furthermore, we can tune the $m + n$ continuous degrees of freedom of the mesh, which are indicated in Fig.4.3.D.

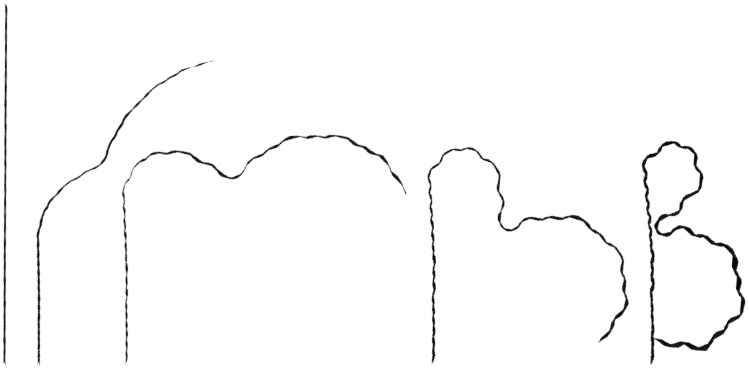

FIGURE 4.5: Side-view of the folding process leading up to the final 3D shape depicted in Fig. 4.4.B, 3D folded shapes calculated using software from [63]. A movie illustrating the folding process can be found online.

4.4 Designing Origami Sheets with Two Target Shapes

The strategy explained in the previous section can be extended to tune the shape of both folding branches of a class-I tiling. An example of this is shown in Fig.4.6.A, where we show a class-I brick tiling. We can choose any pattern of A, B and F tiles on both the top and the left edge. The rest of the $(m-1)(n-1)$ tiles in the pattern, masked by a partially translucent layer, are fixed by this choice. Note that the resultant pattern also contains C tiles in the interior. These are located wherever we find a F tile on the left edge in the corresponding row, and top edge in the corresponding column.

In Fig.4.6.B we show a realization of the tiling of Fig.4.6.A. The mountain valley pattern here is the one that corresponds to the vertically corrugated folding branch. A 3D visualization of this MV pattern is depicted in Fig.4.6.C. Contrastingly, Fig.4.6.D depicts the same quadrilateral mesh as in Fig.4.6.B, but with the mountain valley pattern of the horizontally corrugated folding branch. A 3D visualization of the folded state of this

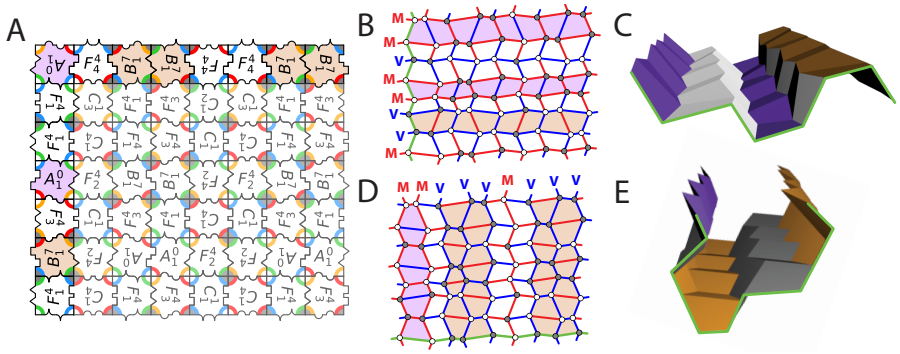

FIGURE 4.6: (A) A 7 by 8 tile class-I tiling, containing all 10 A, B, C_i, and F_i tiles. (B) Horizontally corrugated shape, where the sign of the folds along each row is identical. (C) 3D visualization of the mesh shown in (B). (D) Vertically corrugated shape, where the sign of the folds along each column is identical. (E) 3D visualization of the mesh shown in (D). 3D folded shapes in (D,E) calculated using software from [63]. Green lines in (B,C) and (D,E) are a visual aid to indicate the orientation of the patterns in their flat and folded configurations.

MV pattern is depicted Fig.4.6.E. Clearly, the pattern of tiles along the left edge determines the curvature pattern of one folding branch; the pattern along the top edge determines the curvature pattern of the other folding branch. Hence, this strategy allows to independently design two 3D shapes.

To illustrate the possibilities of this combinatorial origami design, we designed a 38 $\times$ 38 class I brick pattern, shown in Fig. 4.7. Here the A and B-tiles are highlighted in purple and orange (respectively), to indicate the areas where the corresponding crease pattern will develop curvature. In Fig. 4.8.A we show the resulting crease pattern, using a base vertex with angles $\alpha_i = \{60°, 105°, 120°, 75°\}$. This pattern was designed with two target shapes: the letter α, and the letter ω. The bottom edge of this pattern (indicated in red) folds into the shape of the letter 'α' when folded along the horizontal direction, as can be seen in the computer visualization in Fig. 4.8.B, and the rest of sheet is an extrusion of this shape. When folded along the vertical direction, the left edge of this pattern (indicated in green) folds into the shape of the letter 'ω', as can be seen in the computer visualization in Fig. 4.8.D.

To demonstrate that this strategy works to fold sheets of material into

multiple different target shapes, we lasercut the pattern in Fig. 4.8 into two 50 cm by 60 cm Mylar™ sheets, with a thickness of 0.2 mm. Here we program the laser cutter to scorch the crease pattern 0.1 mm deep into the sheet. These two identical sheets are then manipulated by hand to into

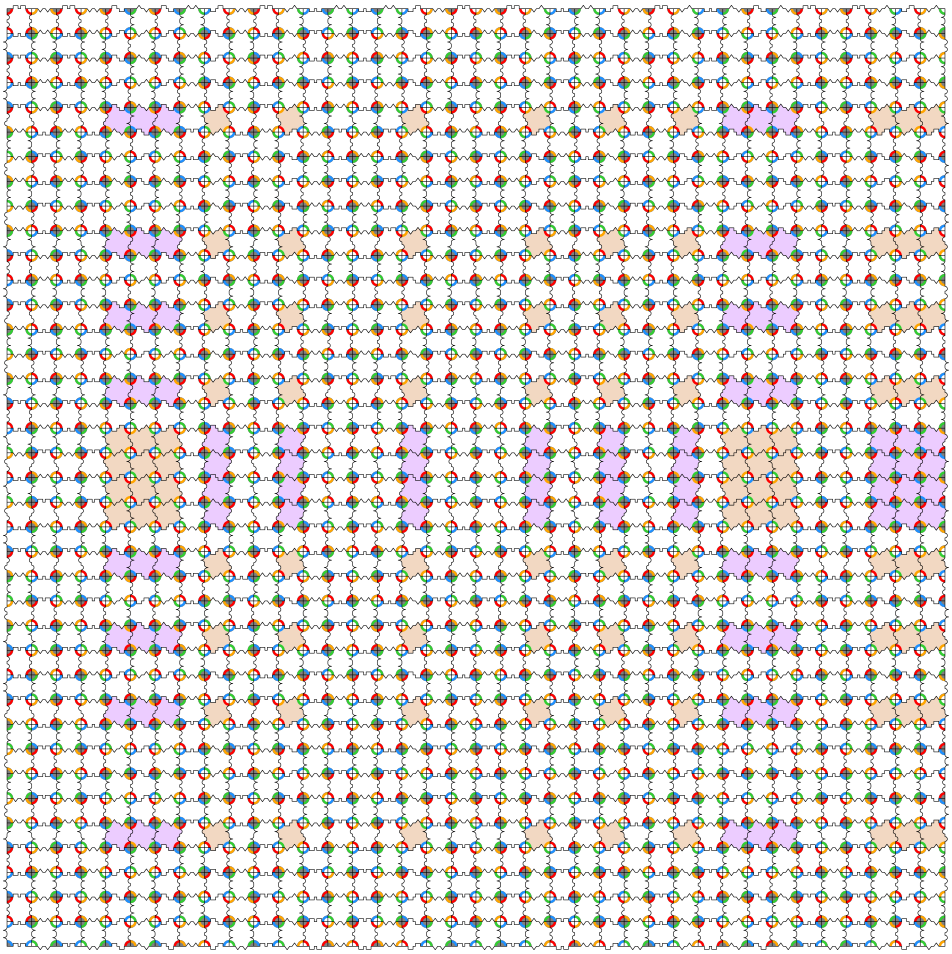

FIGURE 4.7: Brick pattern corresponding to the crease pattern shown in Fig. 4.8.A, where the letters indicating the brick type are omitted. A-tiles are highlighted in purple, whereas B-tiles are highlighted in orange. We encourage the reader to download the high-resolution version of this image.

the two different target shapes. Final folded shapes are shown in Fig.4.8.C and Fig.4.8.E. We note the close resemblance to the shapes in the computer simulations of Fig.4.8.B,D. Finally, we note that the shapes depicted in Fig. 4.8.C,E share the same underlying 2D structure, and it is therefore

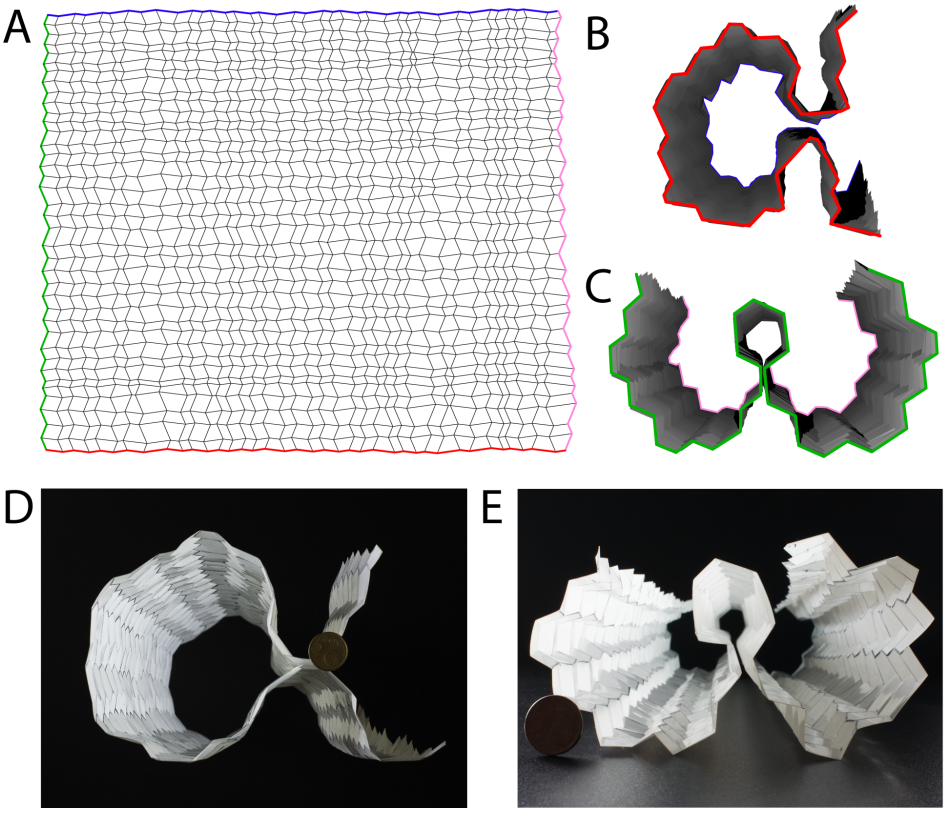

FIGURE 4.8: (A) A 38 by 38 tile class-I (37 by 37 internal vertices) class-I tiling, created from the brick pattern shown in Fig. 4.7, with $\alpha_i = \{60°, 105°, 120°, 75°\}$. (B) 3D visualization of the final folded state of the pattern displayed in (A) when folded in the horizontal direction, representing the letter 'α'. (C) Lasercut Mylar™ sheet, folded into the same shape as in (B). Five cent euro coin for scale. (D) 3D visualization of the final folded state of the pattern displayed in (A) when folded in the vertical direction, representing the letter 'ω'. (E) Lasercut Mylar™ sheet, folded into the same shape as in (D). Five cent euro coin for scale. 3D folded shapes in (B,D) calculated using software from [63].

in principle possible for the shape of Fig. 4.8.B to morph continuously into the shape depicted in Fig. 4.8.C (via the flat, unfolded state). Movies illustrating the folding process of both shapes are available for download.

We conclude that our design strategy allows us to create a single 2D crease pattern, which has two mountain valley patterns with corresponding 3D shapes. Both of these shapes can be tuned such that they have an arbitrary mountain-valley arrangement along one direction. This allows for the creation of multishape origami patterns, which is new in origami design, where usually one only targets a single shape [17–19, 34, 64, 65].